

## **INTERNAL CURING AND MICROSTRUCTURE OF HIGH-PERFORMANCE MORTARS**

Dale P. Bentz and Paul E. Stutzman  
Building and Fire Research Laboratory  
National Institute of Standards and Technology  
100 Bureau Drive, Stop 8615  
Gaithersburg, MD 20899-8615  
PHONE: (301)975-5865  
FAX: (301) 990-6891  
[dale.bentz@nist.gov](mailto:dale.bentz@nist.gov), [paul.stutzman@nist.gov](mailto:paul.stutzman@nist.gov)

**Biography:** ACI member **Dale P. Bentz** is a Chemical Engineer in the Materials and Construction Research Division, National Institute of Standards and Technology (NIST), Gaithersburg, MD. He received his B.S. in Chemical Engineering from the University of Maryland and his M.S. in Computer and Information Science from Hood College. He is a member of ACI Committees 231 (Early Ages), 236 (Materials Science), and 308 (Curing). His research interests include experimental and computer modeling studies of the microstructure and performance of materials.

**Paul E. Stutzman** is a Physical Scientist in the Materials and Construction Research Division at NIST. He received his A.B. in Geology from Hanover College and his M.S. in Geology from Southern Illinois University at Carbondale. His research interests include the development and application of techniques for characterizing material microstructure, and he manages the division's microstructure laboratory. He is active in both ASTM C01 and C09 committees on cement and concrete.

### **ABSTRACT**

While typically used to reduce early-age autogenous shrinkage and cracking, internal curing will also strongly influence the microstructure that is produced in cement-based materials. In this paper, the microstructure of a set of three different blended cement high performance mortars produced with and without internal curing will be compared. For these mortars with a water-to-cementitious materials ratio of 0.3 by mass, internal curing has been provided by the addition of pre-wetted lightweight fine aggregates. Their microstructures have been examined after 120 days of sealed curing using scanning electron microscopy of polished surfaces in the back-scattered electron imaging mode. Clear distinctions between the microstructures produced with and without internal curing are noted, including differences in the unreacted cementitious content, the porosity, and the microstructure of the interfacial transition zones between sand grains (normal and lightweight) and the hydrated cement paste. These microstructural observations will be related to previously measured performance attributes such as autogenous deformation and compressive strength development.

**Keywords:** Blended cement; internal curing; hydration; microstructure; porosity; scanning electron microscopy.

## INTRODUCTION

After being suggested by Philleo<sup>1</sup> in 1992, internal curing was employed successfully in the laboratory during the late 1990s to reduce the early-age deformation of high-performance (low water-to-cementitious materials ratio ( $w/cm$ )) concretes.<sup>2-4</sup> In this century, this laboratory research has been translated into practical field experience with the successful placement of several high volume concrete projects, including a railway transit yard<sup>5</sup> and a continuously reinforced concrete pavement.<sup>6</sup> By replacing a portion of the normal weight aggregates with pre-wetted lightweight aggregates (LWA), additional internal curing water is provided to the concrete mixture. During the hydration of the cement paste within the concrete mixture, this internal curing water will be drawn from the LWA into the hydrating paste, maintaining a high degree of saturation (water-filled pores) in the cement paste and avoiding or at least reducing self-desiccation stresses and their accompanying autogenous deformations.

The effectiveness of internal curing has been previously quantified in numerous studies, with respect to a variety of measured physical properties including internal relative humidity, autogenous deformation, ring test strains and cracking, degree of hydration, and compressive strength.<sup>2-4,7-11</sup> To date, there have been far fewer direct observations of the influence of internal curing on the microstructure of the hydrating cement paste. The three-dimensional microstructure and water movement from the LWA to the surrounding cement paste have been directly observed during the first few days of hydration using x-ray microtomography.<sup>12</sup> As part of his M.S. thesis,<sup>13</sup> Lam presented a few scanning electron micrographs of concretes with internal curing supplied either via saturated LWA or the addition of superabsorbent polymers. His general conclusion was that “the ITZ (interfacial transition zone) of lightweight aggregate concrete was superior to that of normal weight aggregate concrete due to the interlocking exhibited by paste with the pores at the surface of the aggregates.”<sup>14</sup> This observation is in agreement with the results of Zhang and Gjorv,<sup>15</sup> who observed a dense and homogeneous ITZ between cement paste and lightweight aggregates with a porous outer layer. In this paper, the long term (120 d) microstructures of three different blended cement high-performance mortars with and without internal curing will be compared based on scanning electron microscopy (SEM) analysis. The approach is similar to that presented previously by the authors to compare the long term microstructures of low  $w/cm$  cement pastes cured under sealed and saturated conditions.<sup>16</sup>

## RESEARCH SIGNIFICANCE

Direct observation of the influence of internal curing on the microstructure of the hydrating cement paste should provide support for previous results indicating that internal curing reduces autogenous deformation, increases achieved hydration, and may increase compressive strength.<sup>2-4,7-11</sup> These changes in properties produced by internal curing all suggest that a higher degree of saturation is maintained within the hydrating cement paste. This saturation should in turn directly influence the microstructure, both in terms of the unhydrated cement component and the capillary porosity. Here, scanning electron microscopy is applied to specimens that have been cured for 120 d to examine these microstructural features. The observations are interpreted in terms of previous measurements of autogenous deformation and compressive strength for these mortars.<sup>11</sup>

## EXPERIMENTAL

The materials and mortar mixtures have been described in detail previously,<sup>11</sup> and will only briefly be presented here. High performance mortars ( $w/cm=0.3$ ) with and without internal curing were prepared for three different commercially available blended cements, containing approximately 8 % silica fume (**SF**), 20% slag (**SLAG**), and 25 % Class F fly ash (**FA**) by mass, respectively. Internal curing was provided by the addition of a saturated-surface-dry (SSD) lightweight fine aggregate at a level intended to provide an extra 0.08 units of internal curing water per unit mass of blended cement powder in each mortar mixture.<sup>11</sup> The complete mixture proportions are provided in **Table 1**. From these mixtures, 50 mm mortar cubes and corrugated mortar tubes were prepared for the measurement of compressive strength and autogenous deformation, respectively. All curing was conducted under sealed conditions at 25 °C (77 °F).

### Scanning Electron Microscopy

After the autogenous deformation specimens had been measured for 56 d, their curing was continued under sealed conditions at 25 °C (77 °F) out to 120 d. At that age, small cylindrical specimens several mm thick were cut from the central portion of one tube for each of the six mortars and stored in ethanol for at least one week, to replace any water remaining in the specimens and halt hydration. These pieces were then placed in an ultra low viscosity epoxy to replace the ethanol and cured in an oven at 60 °C (140 °F). After curing, the specimens were prepared for viewing at magnifications of 1200X and 2400X in the SEM as described previously.<sup>17</sup> Representative backscattered electron (BSE) images, each with 1024 x 768 pixels, were acquired for the microstructures achieved after 120 d of sealed curing for each of the six mortars.

## RESULTS

To provide a context in which to consider the microstructural observations, it is useful to first review the previous results that have been obtained with respect to compressive strength and autogenous deformation.<sup>11</sup> Mortar cube compressive strengths were measured on 3 replicate specimens after 3 d, 8 d, 28 d, and 56 d of sealed curing at 25 °C (77 °F), using a mechanical testing machine, at a loading rate of 20.7 MPa/min (3000 psi/min), switching to deformation control once a load of 13.8 MPa (2000 psi) was reached. The strength results for these unconfined mortar cubes<sup>11</sup> are provided in **Table 2**. In every case, while each internally cured mortar exhibits a slightly lower 3-d compressive strength in comparison to its control counterpart, at ages of 8 d and beyond, the compressive strength of those mortars with internal curing generally exceeds that of their corresponding control mortar by about 10 %. This would suggest that the specimens with internal curing have eventually achieved a greater degree of hydration under the sealed curing conditions employed in this study, offsetting any strength reduction due to the incorporation of a porous lightweight aggregate. In addition, in every case, the provision of internal curing resulted in a substantial reduction in the measured autogenous shrinkage for the corrugated tube specimens,<sup>11</sup> suggesting a higher degree of saturation and less self-desiccation in the hydrating cement paste within the internally cured mortar specimens.

The SEM/BSE images for the silica fume blended cement mortars with and without internal curing are provided in **Fig. 1**. In each figure, the two images at the top represent microstructures obtained for the mortar without internal curing while the bottom two images are for the mortar with internal curing via pre-wetted LWA. In the bottom images, one of the highly porous LWA particles is clearly visible (and labeled). In examining the microstructure of the cement paste, it is clear that the internal curing has had several influences. In general, in the lower magnification images, there are fewer residual unhydrated cement particles in the microstructure with internal curing, indicating a greater achieved degree of hydration. Additionally, there are many more “empty” coarse pores present in the microstructure without internal curing, in agreement with the self-desiccation expected in this low  $w/cm$  paste. Many of these empty pores are observed to surround the residual cement grains, commonly referred to as hollow-shell or Hadley grain pores. Previously, significant amounts of such pores have been observed in  $w/cm=0.25$  and  $w/cm=0.40$  blended cement pastes with 10 % silica fume by mass.<sup>18</sup> In the mortar with internal curing, capillary pores in the hydrating cement paste remain water-filled for a longer period of time, at the expense of the even larger pores present in the LWA, and in their saturated state are available to be filled with hydration products. The greater degree of hydration and the absence of these larger empty pores could both contribute to the higher compressive strengths achieved at later ages in the mortars with internal curing. In terms of the observed reduction in autogenous shrinkage, it is the emptying of the much larger pores in the LWA in the case of mortars with internal curing, as opposed to the emptying of much smaller pores in the hydrating cement paste when no internal curing is present that substantially reduces the capillary stresses and resulting measured strains. These microstructural observations are quite consistent with those made previously on  $w/c=0.35$  ordinary portland cement pastes cured under sealed and saturated conditions.<sup>16</sup> A final point worth noting in **Fig. 1** is the presence of a few agglomerated silica fume (middle grey) particles (one of which is labeled), suggesting that the dispersion of the silica fume within this blended cement could perhaps be improved.

**Figure 2** provides the equivalent set of figures for the mortars based on the blended cement containing slag. In this figure, it can be observed that, even after 120 d, the reactivity of the slag particles, as indicated by the thicknesses of the hydration rims surrounding them, is much less than that of the cement particles, in agreement with previous quantitative SEM-based measurements on blended cement pastes containing slag.<sup>19</sup> Once again, the application of internal curing is observed to produce a much denser, more homogeneous cement paste microstructure, with fewer unhydrated cement particles and fewer and smaller empty pores. In the mortar with internal curing, in the figure at the bottom left of **Fig. 2**, there is excellent integrity between the LWA and the nearby cement paste, suggesting an almost continuous ITZ between the hydrating cement paste and the LWA particles, as has been noted previously.<sup>14,15</sup>

Finally, **Fig. 3** provides an equivalent set of figures for the mortars based on the blended cement containing a Class F fly ash. Once again, the internal curing has produced a denser microstructure with fewer and smaller pores. In addition, it appears that there are more and larger regions of calcium hydroxide (CH) in the specimens without internal curing (top images in **Fig. 3**). As this hydrating microstructure self-desiccates, little water will remain to promote the later age pozzolanic reaction of the fly ash particles with the calcium hydroxide produced by the cement hydration reactions. In the specimen with internal curing, this needed water is readily

available even at later ages and thus much of the CH has reacted pozzolanically with the fly ash, so that far fewer regions of CH are visible in the SEM micrographs (bottom images in **Fig. 3**).

In examining additional SEM images at a variety of magnifications, an additional observation was made in the microstructures with internal curing. Even though these mortars were formulated with sufficient overall extra internal curing water to maintain saturation of the cement paste, locally, dense and porous regions of microstructure were noted. The existence of porous and dense regions within the same specimen is similar to previous observations made by Diamond and Landis in conventional (no internal curing) mortars and concretes.<sup>20</sup> It is easy to conjecture that an initially dense region, due to its smaller pore sizes, will imbibe water from a nearby more porous region, further densifying the dense region and assuring that the porous region remains porous, due to a lack of water for continuing hydration. Thus, during self-desiccation, dense regions may become denser while porous regions become relatively more porous, not unlike the old saying that “the rich get richer and the poor get poorer.”

## CONCLUSIONS

The 120 d microstructures of three different blended cement mortars with and without internal curing as observed using SEM/BSE imaging are consistent with previous observations comparing physical properties of these materials. The increased hydration and absence of large empty pores (hollow-shell or partly hollow-shell pores) within the hydrating cement paste may both contribute to the later age strength increases produced by internal curing. The emptying of the larger pores within the LWA as opposed to much smaller pores within the hydrating paste should result in a substantial reduction in the capillary stresses and resulting autogenous shrinkage of the mortars. Ultimately, this may reduce the risk of early-age cracking.

## ACKNOWLEDGEMENTS

The authors would like to thank Northeast Solite Corporation, Lafarge Canada Inc., and Holcim (US) Inc. for providing materials and Dr. Sidney Diamond for a careful review of the manuscript.

## REFERENCES

1. Philleo, R.E., “Concrete Science and Reality,” in Materials Science of Concrete II, J. Skalny and S. Mindess, eds., American Ceramic Society, Westerville, OH, 1991, pp. 1-8.
2. Weber, S., and Reinhardt, H.W., “A New Generation of High Performance Concrete: Concrete with Autogenous Curing,” *Advanced Cement-Based Materials*, V. 6, 1997, pp. 59-68.
3. van Breugel, K., and de Vries, H., “Mixture Optimization of Low Water/Cement Ratio, High-Strength Concretes in View of Reduction of Autogenous Shrinkage,” in Proceedings of the International Symposium on High-Performance and Reactive Powder Concretes, P.C. Aitcin and Y. Delagrange, eds., University of Sherbrooke, Quebec, Canada, 1998, pp. 365-382.
4. Bentur, A., Igarishi, S., and Kovler, K., “Prevention of Autogenous Shrinkage in High Strength Concrete by Internal Curing Using Wet Lightweight Aggregates,” *Cement and Concrete Research*, V. 31, No. 11, 2001, pp. 1587-1591.

5. Villareal, V.H., and Crocker, D.A., "Better Pavements through Internal Hydration," *Concrete International*, V. 29, No. 2, 2007, pp. 32-36.
6. Friggle, T., and Reeves, D., "Using Intermediate Gradations of Rotary Kiln Lightweight Aggregate to Enhance Cement Hydration in Mainline Paving Mix," this proceedings, 2007.
7. Cusson, D., and Hoogeveen, T., "Internally-cured High-performance Concrete under Restrained Shrinkage and Creep," in CONCREEP 7 Workshop on Creep, Shrinkage, and Durability of Concrete and Concrete Structures, Nantes, France, 2005, pp. 579-584.
8. Duran-Herrara, A., Aitcin, P.C., and Petrov, N., "Effect of Saturated Lightweight Sand Substitution on Shrinkage in 0.35 w/b Concrete," *ACI Materials Journal*, V. 104 (1), 2007, pp. 48-52.
9. Lura, P., "Autogenous Deformation and Internal Curing of Concrete," Ph.D. Thesis, Delft Institute of Technology, The Netherlands, 2003.
10. Mack, E.C., "Using Internal Curing to Prevent Concrete Bridge Deck Cracking," M.S. Thesis, Cleveland State University, June 2006.
11. Bentz, D.P., "Internal Curing of High-Performance Blended Cement Mortars," accepted by *ACI Materials Journal*, 2007.
12. Bentz, D.P., Halleck, P.M., Grader, A.S., and Roberts, J.W., "Water Movement during Internal Curing: Direct Observation using X-ray Microtomography," *Concrete International*, V. 28, No. 10, 2006, pp. 39-45.
13. Lam, H., "Effects of Internal Curing Methods on Restrained Shrinkage and Permeability," M.Sc. Thesis, University of Toronto, 2005.
14. Lam, H., and Hooton, R.D., "Effects of Internal Curing Methods on Restrained Shrinkage and Permeability," in Proceedings of the 4th International Seminar: Self-Desiccation and Its Importance in Concrete Technology, B. Persson, D. Bentz, and L.-O. Nilsson, eds., Gaithersburg, MD, 2005, pp. 210-228.
15. Zhang, M.-H., and Gjorv, O.E., "Microstructure of the Interfacial Zone between Lightweight Aggregate and Cement Paste," *Cement and Concrete Research*, V. 20, 1990, pp. 610-618.
16. Bentz, D.P., and Stutzman, P.E., "Curing, Hydration, and Microstructure of Cement Paste," *ACI Materials Journal*, V. 103, No. 5, 2006, pp. 348-356.
17. Bentz, D.P., and Stutzman, P.E., "SEM Analysis and Computer Modelling of Hydration of Portland Cement Particles," in *Petrography of Cementitious Materials*, ASTM STP 1215, S.M. DeHayes and D. Stark, eds., American Society for Testing and Materials, Philadelphia, PA, 1994, pp. 60-73.
18. Kjellsen, K.O., and Atlassi, E.H., "Pore Structure of Cement Silica Fume Systems: Presence of Hollow-Shell Pores," *Cement and Concrete Research*, V. 29, 1999, pp. 133-142.
19. Feng, X., Garboczi, E.J., Bentz, D.P., Stutzman, P.E., and Mason, T.O., "Estimation of the Degree of Hydration of Blended Cement Pastes by a Scanning Electron Microscope Point-Counting Procedure," *Cement and Concrete Research*, V. 34, 2004, pp. 1787-1793.
20. Diamond, S., and Landis, E., "Microstructural Features of a Mortar as Seen by Computed Microtomography," *Materials and Structures*, DOI 10.1617/s11527-006-9194-9, 2006.

## TABLES AND FIGURES

### **List of Tables:**

**Table 1** - Mortar mixture proportions used in the study<sup>11</sup>

**Table 2**- Measured mortar cube compressive strengths for the various mixtures.<sup>11</sup>

**List of Figures:**

**Fig. 1 - BSE/SEM images of mortar microstructures for silica fume blended cement without (top) and with (bottom) internal curing at magnifications of 1200X (left) and 2400X (right). Scale bar for each image is located in lower right corner. 25  $\mu\text{m}$  is equivalent to 0.001 in. and 12.5  $\mu\text{m}$  is equivalent to 0.0005 in.**

**Fig. 2 - BSE/SEM images of mortar microstructures for slag blended cement without (top) and with (bottom) internal curing at magnifications of 1200X (left) and 2400X (right). Scale bar for each image is located in lower right corner. 25  $\mu\text{m}$  is equivalent to 0.001 in. and 12.5  $\mu\text{m}$  is equivalent to 0.0005 in.**

**Fig. 3 - BSE/SEM images of mortar microstructures for fly ash blended cement without (top) and with (bottom) internal curing at magnifications of 1200X (left) and 2400X (right). Scale bar for each image is located in lower right corner. 25  $\mu\text{m}$  is equivalent to 0.001 in. and 12.5  $\mu\text{m}$  is equivalent to 0.0005 in.**

**Table 1 - Mortar mixture proportions used in the study<sup>11</sup>**

<b>Material</b>	<b>Control Mixture</b>	<b>Mixture with Internal Curing</b>
Blended cement	2000. g (4.405 lb)	2000. g (4.405 lb)
Water	584.6 g (1.288 lb)	584.6 g (1.288 lb)
Water-reducing admixture (assumed 60 % water by mass)	25.6 g (0.056 lb)	25.6 g (0.056 lb)
F95 fine sand <sup>A</sup>	950. g (1.982 lb)	696.1 g (1.533 lb)
Graded sand (ASTM C 778)	722. g (1.590 lb)	613.2 g (1.351 lb)
20-30 sand (ASTM C 778)	722. g (1.590 lb)	576.9 g (1.271 lb)
GS16 coarse sand <sup>A</sup>	1406. g (3.097 lb)	704.9 g (1.553 lb)
SSD LWA	---	833.7 g (1.836 lb)
Water in SSD LWA	---	160. g (0.352 lb)

<sup>A</sup>F95 and GS16 correspond to sand supplier designations.

**Table 2- Measured mortar cube compressive strengths for the various mixtures.<sup>11</sup>**

<b>Mixture</b>	<b>3 d strength (MPa)</b>	<b>8 d strength (MPa)</b>	<b>28 d strength (MPa)</b>	<b>56 d strength (MPa)</b>
<b>SF – Control</b>	68.1 (2.0) <sup>B</sup> 9878 psi	80.4 (3.0) 11665 psi	-----	98.0 (2.7) 14232 psi
<b>SF – Internal curing</b>	67.9 (4.6) 9843 psi	87.9 (4.6) 12743 psi	-----	105.6 (6.9) 15312 psi
<b>SLAG – Control</b>	60.9 (0.9) 8827 psi	71.5 (2.0) 10376 psi	81.8 (3.2) 11863 psi	84.3 (5.7) 12226 psi
<b>SLAG – Internal curing</b>	59.2 (4.2) 8581 psi	71.7 (2.3) 10399 psi	88.8 (3.9) 12873 psi	94.6 (1.0) 13729 psi
<b>FA – Control</b>	58.0 (0.5) 8407 psi	70.5 (3.3) 10224 psi	85.3 (3.4) 12365 psi	95.3 (4.0) 13827 psi
<b>FA – Internal curing</b>	57.4 (2.3) 8324 psi	67.5 (3.5) 9794 psi	92.9 (3.8) 13471 psi	101.1 (2.9) 14665 psi

<sup>B</sup>Numbers in parentheses indicate measured standard deviation in MPa for compressive strengths of three replicate cubes at each age for each mixture.

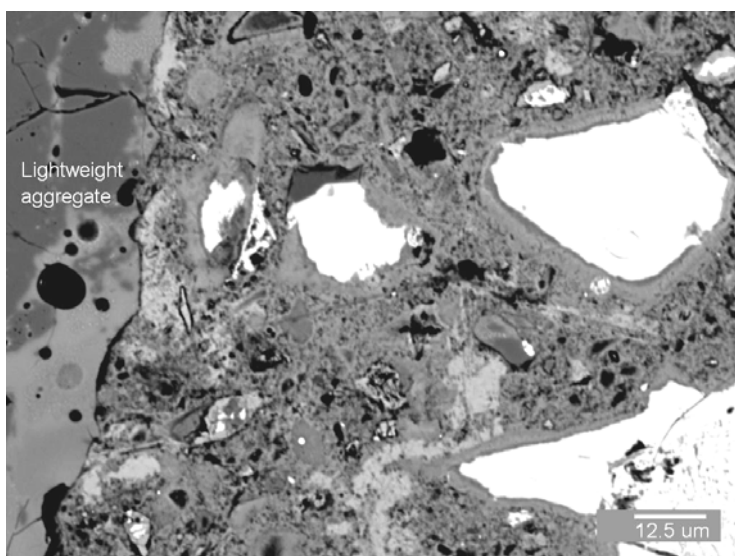
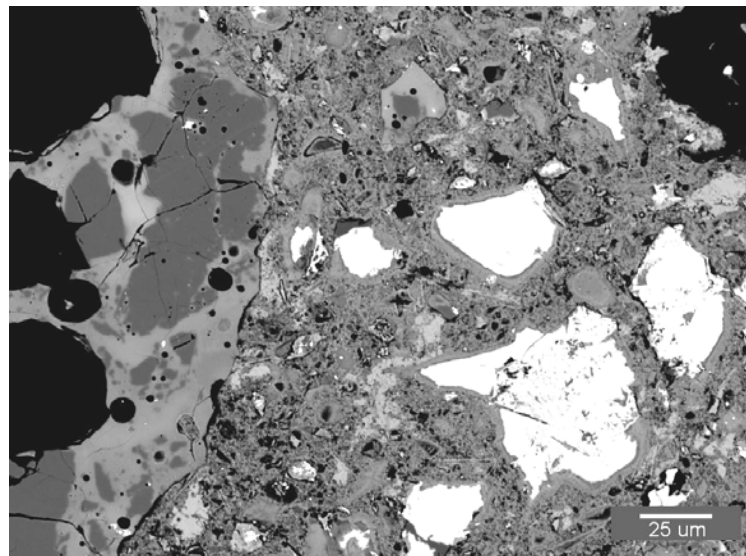
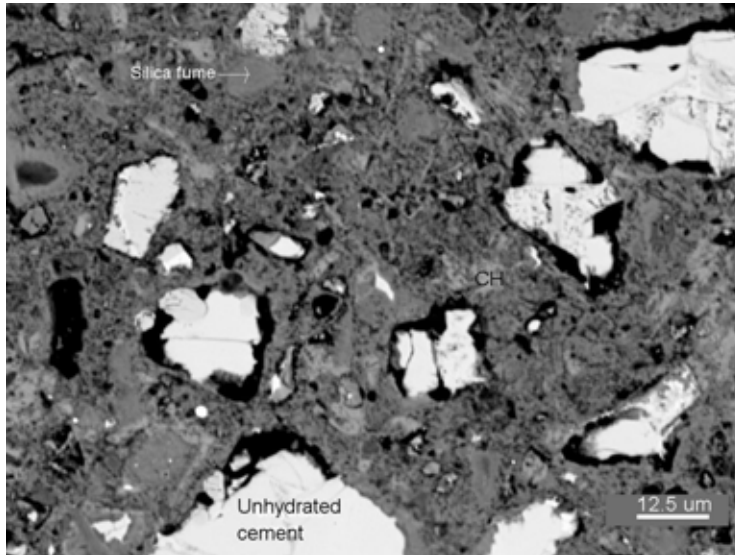
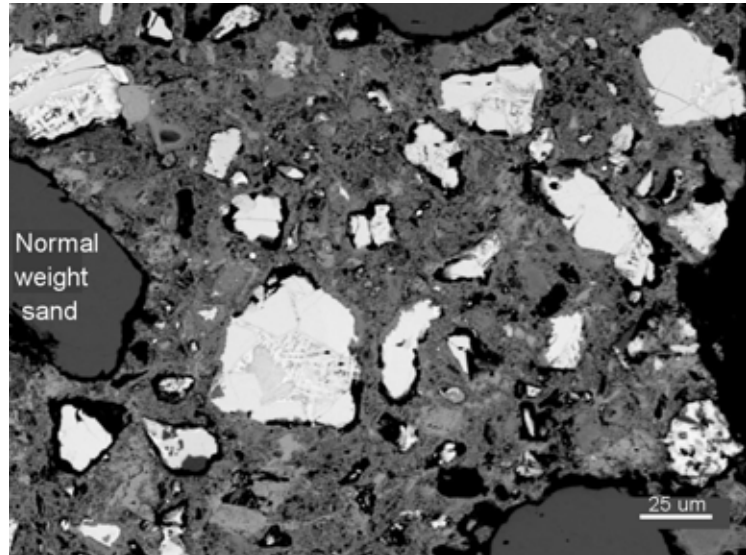


Fig. 1 - BSE/SEM images of mortar microstructures for silica fume blended cement without (top) and with (bottom) internal curing at magnifications of 1200X (left) and 2400X (right). Scale bar for each image is located in lower right corner. 25 μm is equivalent to 0.001 in. and 12.5 μm is equivalent to 0.0005 in.

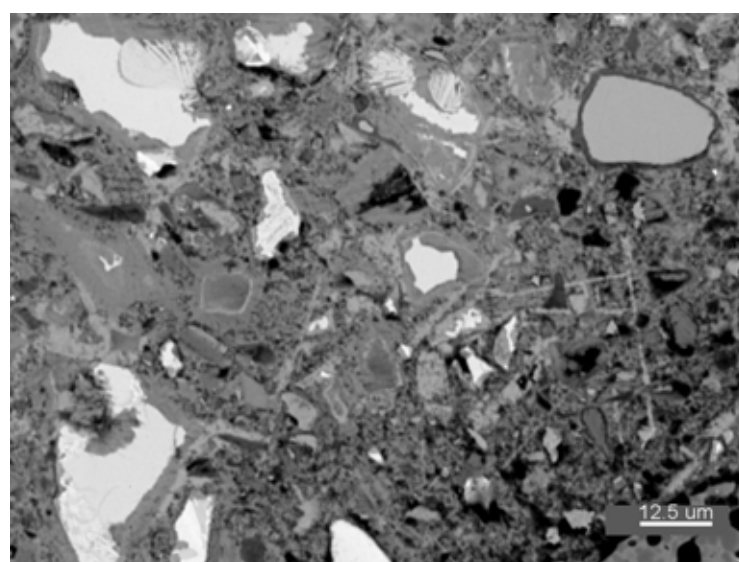
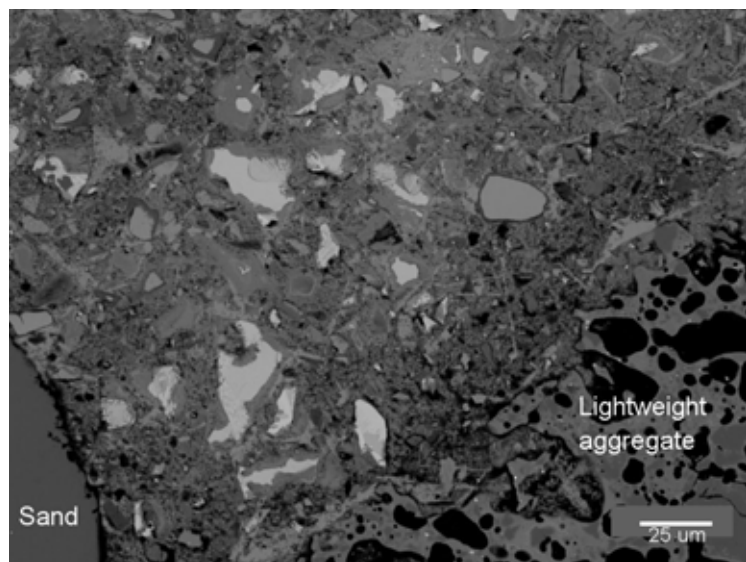
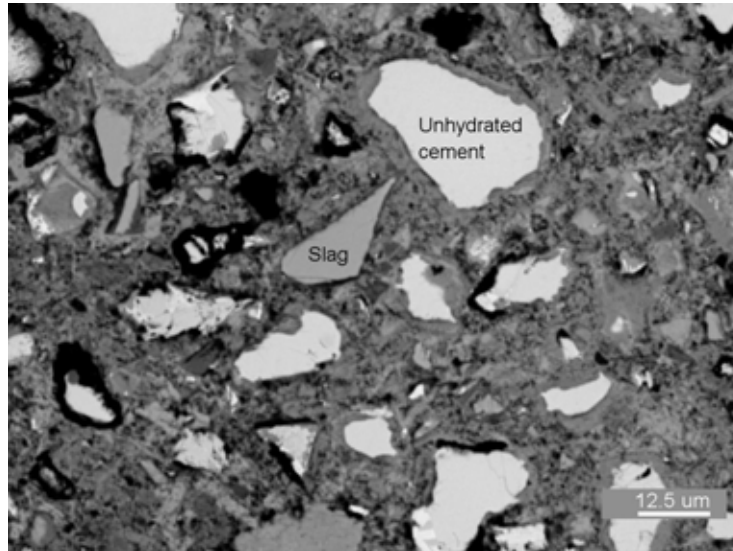
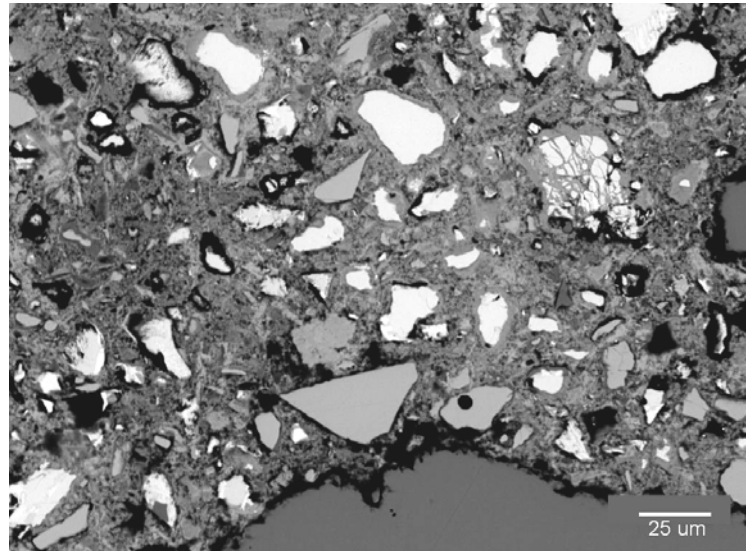


Fig. 2 - BSE/SEM images of mortar microstructures for slag blended cement without (top) and with (bottom) internal curing at magnifications of 1200X (left) and 2400X (right). Scale bar for each image is located in lower right corner. 25 μm is equivalent to 0.001 in. and 12.5 μm is equivalent to 0.0005 in.

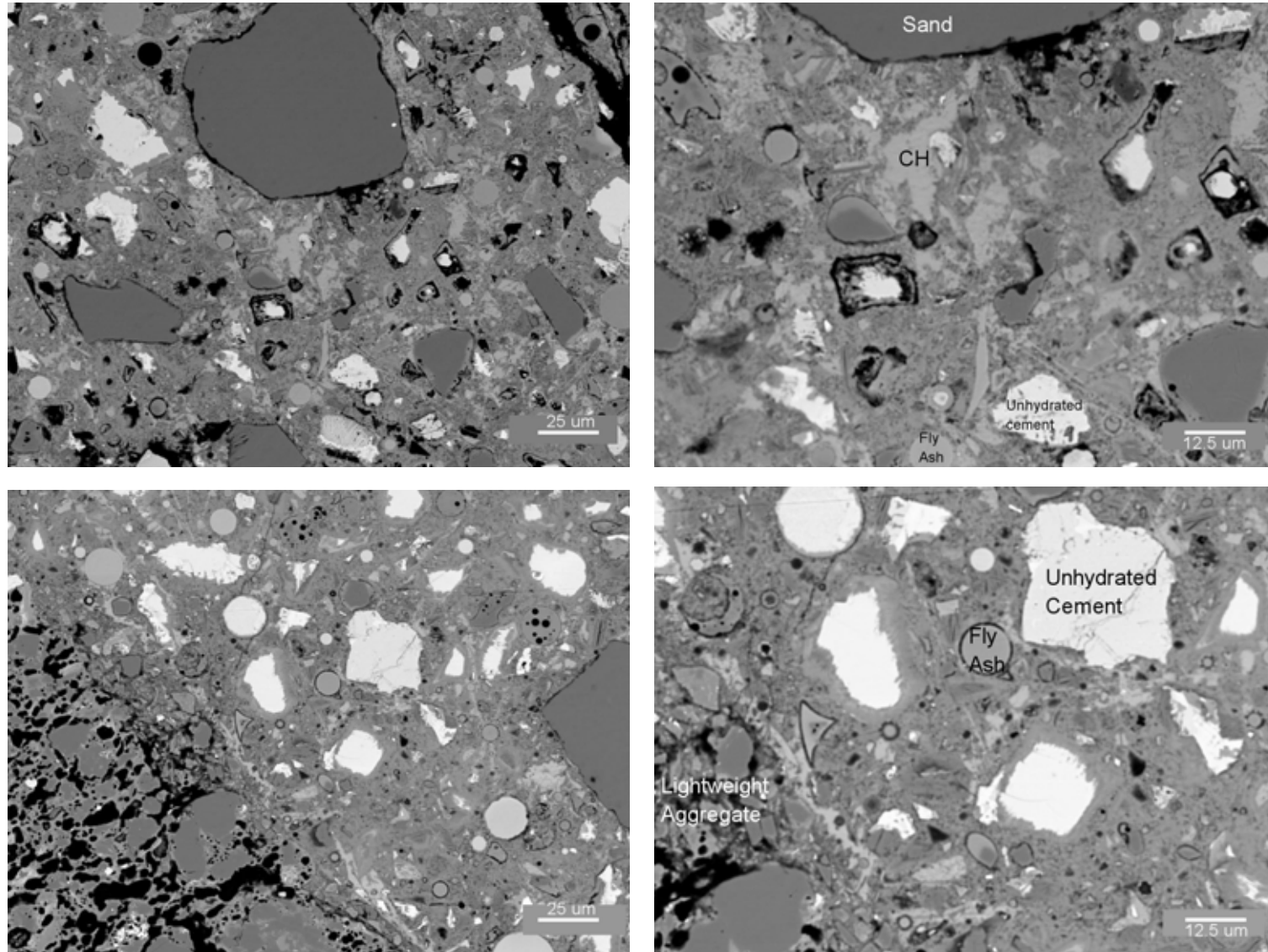


Fig. 3 - BSE/SEM images of mortar microstructures for fly ash blended cement without (top) and with (bottom) internal curing at magnifications of 1200X (left) and 2400X (right). Scale bar for each image is located in lower right corner. 25  $\mu\text{m}$  is equivalent to 0.001 in. and 12.5  $\mu\text{m}$  is equivalent to 0.0005 in.